LETTERS
PUBLISHED ONLINE: 4 SEPTEMBER 2011 | DOI: 10.1038/NNANO.2011.146
nature nanotechnology

Graphene plasmonics for tunable terahertz metamaterials

Long Ju[1], Baisong Geng[1,6], Jason Horng[1], Caglar Girit[1], Michael Martin[2], Zhao Hao[2,3], Hans A. Bechtel[2], Xiaogan Liang[4], Alex Zettl[1,5], Y. Ron Shen[1,5] and Feng Wang[1,5]*

Plasmons describe collective oscillations of electrons. They have a fundamental role in the dynamic responses of electron systems and form the basis of research into optical metamaterials[1–3]. Plasmons of two-dimensional massless electrons, as present in graphene, show unusual behaviour[4–7] that enables new tunable plasmonic metamaterials[8–10] and, potentially, optoelectronic applications in the terahertz frequency range[8,9,11,12]. Here we explore plasmon excitations in engineered graphene micro-ribbon arrays. We demonstrate that graphene plasmon resonances can be tuned over a broad terahertz frequency range by changing micro-ribbon width and *in situ* electrostatic doping. The ribbon width and carrier doping dependences of graphene plasmon frequency demonstrate power-law behaviour characteristic of two-dimensional massless Dirac electrons[4–6]. The plasmon resonances have remarkably large oscillator strengths, resulting in prominent room-temperature optical absorption peaks. In comparison, plasmon absorption in a conventional two-dimensional electron gas was observed only at 4.2 K (refs 13,14). The results represent a first look at light–plasmon coupling in graphene and point to potential graphene-based terahertz metamaterials.

Graphene is an attractive two-dimensional (2D) carbon material. Electrons in graphene behave like massless Dirac fermions and exhibit many exotic physical phenomena, ranging from an anomalous quantum Hall effect[15,16] and Klein tunnelling[17,18] in electrical transport to a universal absorption constant[19,20] and tunable interband transitions[21,22] in optical response. Most of these phenomena are well accounted for by single-particle excitation of electrons. Plasmons in graphene, on the other hand, describe collective excitations of 2D massless electrons. Previous studies established that plasmons have an important role in graphene electron dynamics[23] and lead to new composite excitations in the form of plasmarons[24]. Plasmon resonances in graphene have also been probed using inelastic electron scattering spectroscopy[25,26] and inelastic scanning tunnelling microscopy[27]. However, the fundamental behaviour of light–plasmon coupling in graphene is little known, and the exciting opportunity to design terahertz metamaterials[1–3] using patterned graphene structures has not been explored.

Here we report the first study of tunable plasmon excitations and light–plasmon coupling at terahertz frequencies in graphene micro-ribbon arrays. A micro-ribbon array is the simplest form of sub-wavelength infrared metamaterials. Plasmon excitations in such arrays correspond to collective oscillations of electrons across the width of micro-ribbons. We show that such plasmon excitations can be controlled through micro-ribbon width (w) where plasmon frequency scales as $w^{-1/2}$. This scaling is characteristic of two-dimensional electron gases (2DEGs)[5,6,13,14] and distinctly different from that of bulk plasmons. For a given micro-ribbon array, plasmon resonance can be further tuned *in situ* using electrostatic gating. Plasmon frequency varies with carrier concentration (n) as $n^{1/4}$, a signature of massless Dirac electrons[4–6]. Comparisons between experimental plasmon frequencies and simulation results yield an effective dielectric screening κ of 5 in our devices. The observed light–plasmon coupling from massless electrons in graphene is remarkably strong: the integrated oscillator strength of graphene plasmons is an order of magnitude larger than that achieved in conventional 2D electron systems[13,14]. Hence, graphene plasmon excitations lead to prominent terahertz absorption peaks at room temperature, but low temperatures (4.2 K) were required to measure plasmon absorption in conventional 2DEGs[13,14]. The strong and tunable plasmon–light interaction, together with the excellent electrical properties of graphene and its compatibility with micro/nanofabrication, holds great promise for graphene-based terahertz metamaterials and optoelectronic devices.

Electromagnetic radiation cannot couple to plasmon excitations in homogeneous graphene sheets, but can readily excite plasmon resonances in engineered graphene structures with dimensions much smaller than light wavelengths. In our study we used a simple form of metamaterial made up of periodic graphene micro-ribbon arrays illustrated in Fig. 1a (not to scale) for terahertz plasmon excitations. Ribbon width varied from 1 to 4 μm and gap and ribbon width ratio was maintained at 1:1. We controlled the carrier concentration in graphene ribbon arrays using an ion-gel top gate[28], which allows a large doping range through electrostatic gating. Figure 1b shows the schematic side view of a typical gated device. The atomic force microscopy (AFM) image of a micro-ribbon array sample with a 4 μm ribbon width and its gate-dependent electrical resistance trace are shown in Fig. 1c, d, respectively. The device has a charge neutral point (CNP) at 0.2 V top gate voltage (V_g), and our samples have mobilities around 1,000 $cm^2\ V^{-1}\ s^{-1}$.

We studied plasmon resonances and light–plasmon coupling in graphene micro-ribbon arrays using polarized Fourier transform infrared spectroscopy. Infrared absorption from doped charge carriers is directly related to $-\Delta T/T_{CNP}$, the gate-induced decrease of transmission through graphene micro-ribbon arrays. Here T_{CNP} is the transmission coefficient at CNP and $\Delta T = T - T_{CNP}$. The $-\Delta T/T_{CNP}$ spectra of a gated 4 μm sample ($V_g = -2.0$ V) for terahertz radiation polarized parallel and perpendicular to the ribbons are shown in Fig. 1e and f, respectively.

For incident light polarized along the ribbons, the electrical response of charge carriers is similar to that of free electrons in a

[1]Department of Physics, University of California at Berkeley, Berkeley, California 94720, USA, [2]Advanced Light Source Division, Lawrence Berkeley National Laboratory, Berkeley, California 94720, USA, [3]Earth Sciences Division, Lawrence Berkeley National Laboratory, Berkeley, California 94720, USA, [4]Molecular Foundry, Lawrence Berkeley National Laboratory, Berkeley, California 94720, USA, [5]Materials Science Division, Lawrence Berkeley National Laboratory, Berkeley, California 94720, USA, [6]School of Physical Science and Technology, Lanzhou University, Lanzhou 730000, China.
*e-mail: fengwang76@berkeley.edu

Report Documentation Page

Form Approved
OMB No. 0704-0188

1. REPORT DATE	2. REPORT TYPE	3. DATES COVERED
OCT 2011		**00-00-2011 to 00-00-2011**

4. TITLE AND SUBTITLE	5a. CONTRACT NUMBER
Graphene plasmonics for tunable terahertz metamaterials	5b. GRANT NUMBER
	5c. PROGRAM ELEMENT NUMBER
6. AUTHOR(S)	5d. PROJECT NUMBER
	5e. TASK NUMBER
	5f. WORK UNIT NUMBER
7. PERFORMING ORGANIZATION NAME(S) AND ADDRESS(ES) **University of California at Berkeley,Department of Physics,Berkeley,CA,94720**	8. PERFORMING ORGANIZATION REPORT NUMBER
9. SPONSORING/MONITORING AGENCY NAME(S) AND ADDRESS(ES)	10. SPONSOR/MONITOR'S ACRONYM(S)
	11. SPONSOR/MONITOR'S REPORT NUMBER(S)

12. DISTRIBUTION/AVAILABILITY STATEMENT
Approved for public release; distribution unlimited

13. SUPPLEMENTARY NOTES

14. ABSTRACT

15. SUBJECT TERMS

16. SECURITY CLASSIFICATION OF:			17. LIMITATION OF ABSTRACT	18. NUMBER OF PAGES	19a. NAME OF RESPONSIBLE PERSON
a. REPORT **unclassified**	b. ABSTRACT **unclassified**	c. THIS PAGE **unclassified**	**Same as Report (SAR)**	**5**	

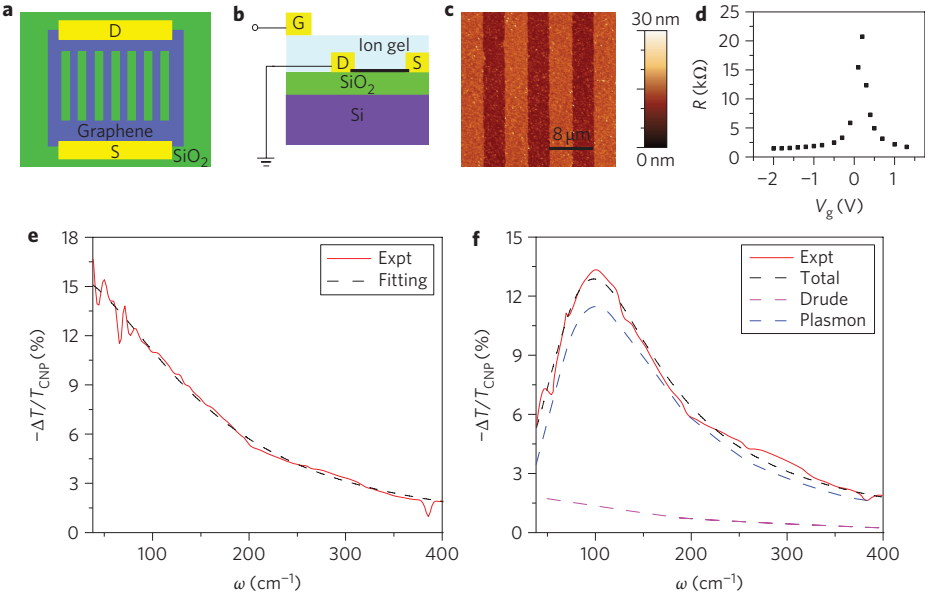

Figure 1 | Plasmon resonance in gated graphene micro-ribbon arrays. a, Top-view illustration of a typical graphene micro-ribbon array. The array was fabricated on transferred large-area CVD graphene using optical lithography and plasma etching. **b**, Side view of a typical device incorporating the graphene micro-ribbon array on a Si/SiO_2 substrate. The carrier concentration in graphene is controlled using the ion-gel top gate. **c**, AFM image of a graphene micro-ribbon array sample with a ribbon width of 4 μm and a ribbon and gap width ratio of 1:1. **d**, Gate-dependent electrical resistance of this graphene micro-ribbon array. The resistance has a maximum at charge neutral point $V_{CNP} = 0.2$ V. **e**,**f**, Gate-induced change of transmission spectra, $-(T - T_{CNP})/T_{CNP}$ (red solid line), with incident light polarized parallel (**e**) and perpendicular (**f**) to the ribbon length, respectively. The gate voltage was set at $V_g = -2$ V. For parallel polarization in **e**, the response originates from free carrier oscillation and can be well reproduced by a Drude fit (black dashed line). For perpendicular polarization in **f**, the spectrum shows a prominent absorption peak at 3 THz (1 THz = 33.3 cm^{-1}) because of plasmon excitation. Plasmon resonance is characterized by a Lorentzian lineshape (blue dashed line). A small free carrier contribution described by Drude absorption (magenta dashed line) is also present as a result of graphene absorption outside the fabricated micro-ribbon array area. The plasmon absorption of over 13% is remarkably strong, and its integrated oscillator strength is more than an order of magnitude larger than that achieved in 2DEGs in conventional semiconductors.

homogeneous graphene sheet, and the spectral shape is well described by the Drude model as $\mathrm{Im}(-1/(\omega + i\Gamma_D))$ (black dashed line in Fig. 1e) with a scattering rate Γ_D of 4 THz. This Drude absorption decreases monotonically with frequency ω. For incident light polarized perpendicular to the ribbon, the resulting spectrum is completely different: an absorption peak originating from plasmon oscillation dominates the optical response (Fig. 1f). This plasmon absorption lineshape can be described by a damped oscillator as $\mathrm{Im}(-\omega/(\omega^2 - \omega_p^2 + i\omega\Gamma_p))$ (blue dashed line) with a plasmon resonance ω_p of 3 THz and a spectral width Γ_p of 4 THz. There is also a small background contribution from the free carrier absorption (magenta dashed line) because part of the infrared beam transmits through unpatterned graphene around the micro-ribbon array. The light–plasmon coupling in graphene is remarkably strong, with over 13% absorption at the plasmon resonance for one doped carbon monolayer. The observed plasmon resonance linewidth is similar to the Drude scattering rate for parallel light polarization, suggesting that plasmon broadening is largely limited by the same scattering processes affecting electrical transport.

The light–plasmon coupling in graphene is remarkably strong compared with that in conventional 2DEGs in semiconductors, and arises from both the small effective electron mass and the efficient electrical gating in graphene. In conventional 2DEGs, the field-induced carrier concentration is limited to $\sim 1 \times 10^{12}$ cm^{-2} to avoid semiconductor dielectric breakdown. At this carrier density, the effective mass of an electron at Fermi energy is 0.02 m_0 in graphene. This electron effective mass is 3.5 (13) times smaller than that in GaAs (Si), and the integrated plasmon oscillator strength is correspondingly larger. In addition, graphene can be gated much more efficiently to over 1×10^{13} cm^{-2} because of its excellent chemical stability and compatibility with different gating configurations. The resulting light–plasmon coupling in graphene can be an order of magnitude stronger than that achieved in conventional 2DEGs, and enabled us to observe terahertz plasmon resonance for the first time at room temperature.

The plasmon resonance in graphene micro-ribbon arrays can be tuned *in situ* by electrostatic doping. For simplicity, we will focus on the hole-doping regime. We determine the gate-induced Fermi energy shift and carrier concentration in graphene through interband optical transitions[21,22]. This is based on the effect that interband transitions can be blocked up to $2|E_F|$ energy in hole-doped graphene as a result of empty initial states. Figure 2a shows gate-induced changes of interband transmission spectra in the 3,000–9,000 cm^{-1} spectral range at different gate biases. Increased infrared transmission is observed up to a threshold energy that shifts to higher values with increased doping. This threshold energy is at $2|E_F|$ (refs 21,22), from which carrier concentration can be deduced by $n = (|E_F|/\hbar v_F)^2/\pi$ (refs 15,16). Plasmon excitations in the graphene micro-ribbon array can be varied by electrical gating, as shown in Fig. 2b for absorption of perpendicularly polarized light. Prominent plasmon absorption peaks are observed, which shift to higher energies and gain oscillator strength with increased carrier concentration. For comparison, we show (in the inset of Fig. 2b) free carrier absorption spectra at different gate voltages (probed with light polarized parallel to micro-ribbons). The spectral shape remains the same in all spectra, although the oscillator strength increases with carrier concentration.

Plasmon excitations in graphene micro-ribbon arrays can also be controlled by engineering the ribbon width. Figure 2c shows AFM images of three micro-ribbon arrays with 1, 2 and 4 μm ribbon widths, respectively, and Fig. 2d shows $-\Delta T/T_{CNP}$ spectra for the three structures. All spectra were taken at the same hole-doping

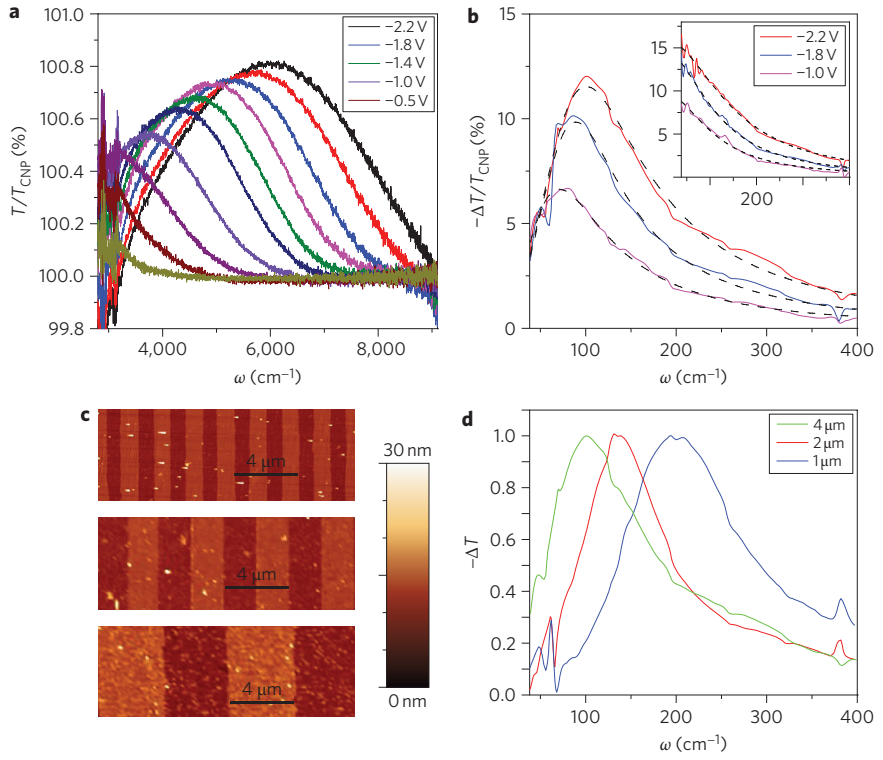

Figure 2 | Control of plasmon resonance through electrical gating and micro-ribbon width. a, Mid-infrared transmission spectra, T/T_{CNP}, of the graphene ribbon array in Fig. 1 as gate voltage $V_g - V_{CNP}$ varies from −0.3 to −2.2 V. The voltages corresponding to the unlabelled lines, starting with the red line and alternating downwards, are: −2.0 V, −1.6 V, −1.2 V, −0.7 V and −0.3 V. On electrical gating, optical transmission is increased up to a threshold energy of $2|E_F|$ as a result of blocked interband optical transitions. This threshold energy provides direct determination of Fermi energy E_F and carrier concentration $n = (|E_F|/\hbar v_F)^2/\pi$ in gated graphene. **b**, Control of terahertz resonance of plasmon excitations through electrical gating. Terahertz radiation was polarized perpendicular to the graphene ribbons. The plasmon resonance shifts to higher energy and gains oscillator strength with increased carrier concentration. For comparison, the inset shows corresponding spectra due to free carrier absorption for terahertz radiation polarized parallel to the ribbons. For this polarization, absorption strength increases with carrier concentration, but spectral shape remains the same. **c**, AFM images of samples with micro-ribbon widths (w) of 1, 2 and 4 μm. **d**, Change of transmission spectra with different graphene micro-ribbon widths for the same doping concentration of 1.5×10^{13} cm^{-2}. The Drude background contributed by unpatterned graphene around the arrays (as in Fig. 1f) was subtracted, and all spectra were normalized by their respective peak values for convenience of comparison. Plasmon resonance frequency ω_p shifts from 3 to 6 THz when micro-ribbon width decreases from 4 to 1 μm.

concentration of 1.5×10^{13} cm^{-2} and were normalized by the respective peak values for convenience of comparison. The plasmon resonance clearly shifts to higher energy with decreasing ribbon widths: resonance frequencies are at 3, 4.1 and 6 THz for ribbon arrays of 4, 2 and 1 μm ribbon widths, respectively. Using nano- and micro-ribbon arrays with a larger range of ribbon widths, terahertz resonance from 1–10 THz can be straightforwardly engineered.

Next we examine the quantitative scaling behaviour of plasmon resonance frequency with carrier concentration and ribbon width. Figure 3a plots plasmon resonance frequencies as a function of $|E_F|$ (or equivalently $|n|^{1/2}$ in the top label) for different micro-ribbon widths. For a given carrier concentration, the plasmon resonance frequencies in different graphene micro-ribbon arrays are described by a scaling behaviour of $\omega_p \propto w^{-1/2}$. This is best shown in Fig. 3b, where all data in Fig. 3a fit into a universal curve once the plasmon resonance frequencies are rescaled by $w^{-1/2}$. This scaling of ω_p with the inverse square root of the relevant spatial dimension is characteristic of 2DEGs[5,6], in contrast to a constant plasmon resonance frequency in bulk plasmons. The universal relation between ω_p and $|E_F|$ in Fig. 3a can also be described by a power-law scaling with $\omega_p \propto |E_F|^{1/2} \propto n^{1/4}$ (solid line). This power-law dependence of $n^{1/4}$ is a signature of massless Dirac electrons[4–6], which is in contrast to $n^{1/2}$ scaling (dashed line) in conventional semiconductors.

A theoretical understanding of the scaling behaviour of plasmon resonance in micro-ribbon arrays can be achieved using the quasi-static description, which is a good approximation for ribbon widths (~1 μm) much smaller than photon wavelengths (~100 μm). The Maxwell equations satisfying the 2D ribbon array boundary conditions can be simplified to

$$\frac{\partial \Phi}{\partial y} = -\frac{2\pi i}{\kappa\omega}\frac{\partial}{\partial x}\left(\sigma^{2D}F(x)\frac{\partial \Phi}{\partial x}\right) \quad (1)$$

where κ is the effective dielectric screening constant, σ^{2D} is the 2D high-frequency conductivity at carrier concentration n, and $F(x)$ is a square function with $F(x) = 1$ at ribbon positions and $F(x) = 0$ in the gap (see Supplementary Information). By introducing dimensionless parameters $X = x/w$ and $Y = y/w$ and using the expression of σ^{2D} for massless Dirac electrons, the above equation can also be expressed as

$$\frac{\partial \Phi}{\partial Y} = \eta\frac{\partial}{\partial X}\left(F(X)\frac{\partial \Phi}{\partial X}\right) \quad (2)$$

with the dimensionless parameter

$$\eta = \frac{2\pi^{1/2}}{\omega(\omega + i\Gamma)}\frac{v_F e^2}{\hbar}\frac{n^{1/2}}{\kappa w}$$

The electrodynamic responses of a micro-ribbon array are uniquely determined by the dimensionless parameter η. Maximum absorption

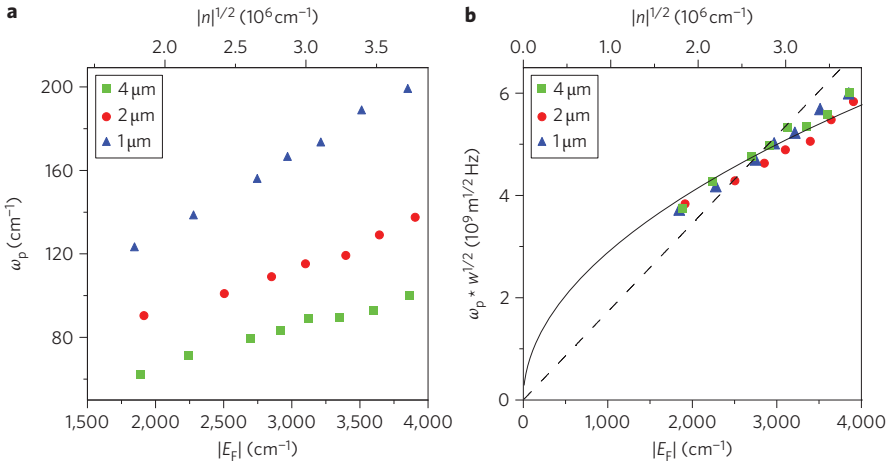

Figure 3 | Scaling laws of graphene plasmon resonance frequency. a, Plasmon resonance frequency ω_p as a function of $|E_F|$ (or equivalently $|n|^{1/2}$ in the top label) for micro-ribbon arrays of different widths. **b**, Plasmon excitation ω_p was normalized by $1/\sqrt{w}$ for micro-ribbon arrays of different widths, which fits all data points (symbols) into a universal curve (solid line). This $w^{-1/2}$ scaling of ω_p is characteristic of 2D electron systems. The universal doping dependence of plasmon resonances is described by a scaling law of $\omega_p \propto |E_F|^{1/2} \propto n^{1/4}$. This $n^{1/4}$ scaling law is a signature of massless Dirac fermions. In comparison, ω_p scales as $n^{1/2}$ (dashed line) in conventional semiconductors.

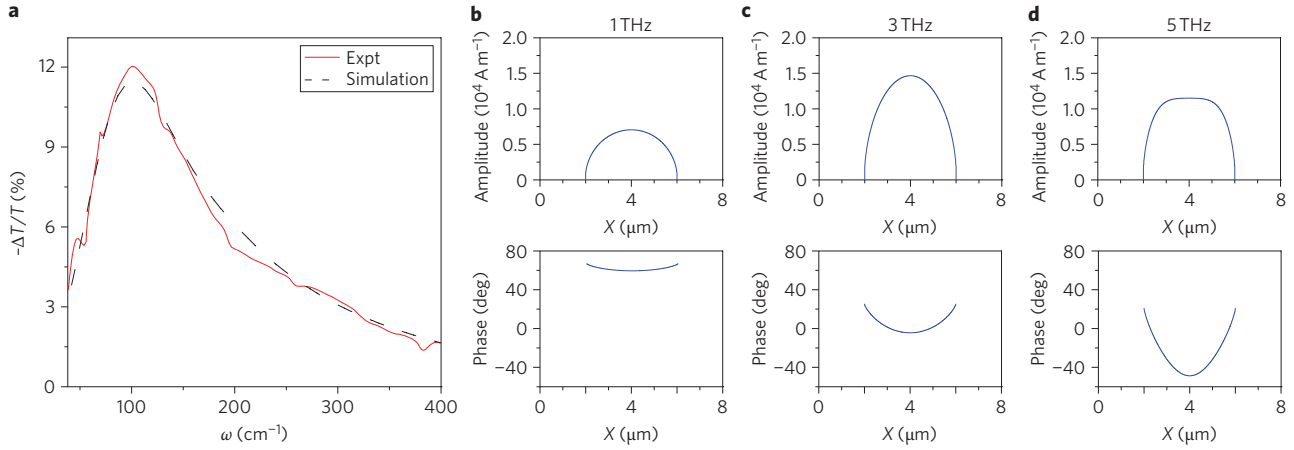

Figure 4 | Simulation of plasmon excitations. a, Transmission change spectrum $-\Delta T/T_{CNP}$ simulated by finite element analysis (dashed line) for the sample in Fig. 1 at carrier concentration of 1.5×10^{13} cm^{-2}. It reproduces well the experimentally observed spectrum (solid line) when the effective environment dielectric constant κ was set as 5, and corresponds to an electron–electron interaction strength of $e^2/\kappa\hbar v_F \approx 0.4$. **b**–**d**, Simulation results for current density amplitude (upper panel) and phase (lower panel) of the device at frequencies below resonance (1 THz, **b**), at resonance (3 THz, **c**) and above resonance (5 THz, **d**). The charge carriers oscillate perpendicular to the graphene ribbons on terahertz irradiation. The oscillating current is highest at the plasmon resonance frequency. The relative phase of the oscillating current with reference to the incident electrical field also varies quickly and changes sign at the resonance frequency. Both are characteristics of a resonant excitation.

of incident light takes place at a specific η value, which determines the plasmon resonance frequency ω_p for given values of w and n. When either ribbon width or carrier concentration changes, plasmon frequency will change accordingly following the scaling behaviour of $\omega_p \propto n^{1/4} \cdot w^{-1/2}$ (for weak damping rate Γ), as observed experimentally.

Although the differential equation readily explains the scaling behaviour of plasmon resonance frequency, it cannot be solved analytically for a quantitative value of ω_p. Instead, we use numerical calculations based on finite element methods to simulate this system, which has only one unknown parameter, namely the dielectric constant κ. Using a κ value of 5, the simulation (dashed line in Fig. 4a) reproduces well the observed $-\Delta T/T_{CNP}$ spectrum for a ribbon width of 4 μm and a doping concentration of 1.5×10^{13} cm^{-2} (solid line in Fig. 4a). The κ value of 5 is reasonable in our devices, given that the terahertz dielectric constants of ion gel, SiO_2 and silicon are 3 (ref. 29), 4 and 11 (ref. 30), respectively. Such a dielectric screening constant will lead to an electron–electron interaction strength of $\alpha_G = e^2/\kappa\hbar v_F \approx 0.4$.

Figure 4b–d plots simulation results for current density amplitudes (top panels) and phases (bottom panels) in the same micro-ribbon array for frequencies below resonance (1 THz), at resonance (3 THz) and above resonance (5 THz), respectively. The current distribution describes electrons oscillating back and forth across the width of graphene micro-ribbons on terahertz radiation. The oscillating current amplitude is largest at the plasmon resonance frequency. Simultaneously, the phase of the current oscillation relative to that of the incident electric field varies quickly and changes sign across the resonance frequency. Both behaviours are typical characteristics of resonance excitation.

Our studies show that plasmon resonances in graphene can be controlled in structure-engineered graphene micro-ribbon arrays,

which represent the simplest form of graphene terahertz metamaterials. Plasmons couple to terahertz radiation strongly, absorbing over 13% at the plasmon resonance for half a monolayer material at room temperature. Peak absorption at resonance can become even stronger with reduced plasmon linewidth, which is currently limited by the scattering rate as in Drude conductivity. We expect that in higher-quality graphene samples, the plasmon linewidth will be reduced in proportion to the increase in mobility. The strong and broadly tunable plasmon resonances observed here in graphene micro-ribbon arrays can be generalized for designing more sophisticated metamaterials based on graphene, and enable new ways of controlling terahertz and far-infrared radiation.

Methods

Large-area graphene was grown using chemical vapour deposition on copper and transferred the graphene sheet onto a Si/SiO_2 wafer following ref. 31. Au/Cr electrodes of 50 nm thickness were deposited onto the graphene sheet in vacuum using stencil masks. Micro-ribbon arrays were fabricated in a 2.5×2.5 mm^2 area at the centre of the graphene sheet using standard optical lithography followed by oxygen plasma etching.

Infrared transmission measurements were performed with a Fourier transform infrared spectrometer at the Advanced Light Source in Lawrence Berkeley National Laboratory. All measurements were performed in 0.1 torr vacuum at room temperature.

Received 27 April 2011; accepted 27 July 2011; published online 4 September 2011

References

1. Yen, T. J. *et al.* Terahertz magnetic response from artificial materials. *Science* **303,** 1494–1496 (2004).
2. Pendry, J. B., Holden, A. J., Stewart, W. J. & Youngs, I. Extremely low frequency plasmons in metallic mesostructures. *Phys. Rev. Lett.* **76,** 4773–4776 (1996).
3. Chen, H. T. *et al.* Active terahertz metamaterial devices. *Nature* **444,** 597–600 (2006).
4. Wunsch, B., Stauber, T., Sols, F. & Guinea, F. Dynamical polarization of graphene at finite doping. *New J. Phys.* **8,** 318 (2006).
5. Polini, M., MacDonald, A. H. & Vignale, G. Drude weight, plasmon dispersion, and pseudospin response in doped graphene sheets. Preprint at http://arXiv.org/abs/0901.4528 (2009).
6. Hwang, E. H. & Das Sarma, S. Dielectric function, screening, and plasmons in two-dimensional graphene. *Phys. Rev. B* **75,** 205418 (2007).
7. Brey, L. & Fertig, H. A. Elementary electronic excitations in graphene nanoribbons. *Phys. Rev. B* **75,** 125434 (2007).
8. Ashkan Vakil & Engheta, N. One-atom-thick IR metamaterials and transformation optics using graphene. Preprint at http://arXiv.org/abs/1101.3585 (2011).
9. Jablan, M., Buljan, H. & Soljacic, M. Plasmonics in graphene at infrared frequencies. *Phys. Rev. B* **80,** 245435 (2009).
10. Koppens, F. H. L., Chang, D. E. & Abajo, F. J. G. d. Graphene plasmonics: a platform for strong light-matter interaction. Preprint at http://arXiv.org/abs/1104.2068v1 (2011).
11. Rana, F. Graphene terahertz plasmon oscillators. *IEEE Trans Nanotechnol.* **7,** 91–99 (2008).
12. Ryzhii, M. & Ryzhii, V. Injection and population inversion in electrically induced p-n junction in graphene with split gates. *Jpn. J. Appl. Phys. 2* **46,** L151–L153 (2007).
13. Allen, S. J., Tsui, D. C. & Logan, R. A. Observation of 2-dimensional plasmon in silicon inversion layers. *Phys. Rev. Lett.* **38,** 980–983 (1977).
14. Batke, E., Heitmann, D. & Tu, C. W. Plasmon and magnetoplasmon excitation in two-dimensional electron space-charge layers on gaas. *Phys. Rev. B* **34,** 6951–6960 (1986).
15. Novoselov, K. S. *et al.* Two-dimensional gas of massless Dirac fermions in graphene. *Nature* **438,** 197–200 (2005).
16. Zhang, Y. B., Tan, Y. W., Stormer, H. L. & Kim, P. Experimental observation of the quantum Hall effect and Berry's phase in graphene. *Nature* **438,** 201–204 (2005).
17. Katsnelson, M. I., Novoselov, K. S. & Geim, A. K. Chiral tunnelling and the Klein paradox in graphene. *Nature Phys.* **2,** 620–625 (2006).
18. Young, A. F. & Kim, P. Quantum interference and Klein tunnelling in graphene heterojunctions. *Nature Phys.* **5,** 222–226 (2009).
19. Mak, K. F. *et al.* Measurement of the optical conductivity of graphene. *Phys. Rev. Lett.* **101,** 246803 (2008).
20. Nair, R. R. *et al.* Fine structure constant defines visual transparency of graphene. *Science* **320,** 1308–1308 (2008).
21. Li, Z. Q. *et al.* Dirac charge dynamics in graphene by infrared spectroscopy. *Nature Phys.* **4,** 532–535 (2008).
22. Wang, F. *et al.* Gate-variable optical transitions in graphene. *Science* **320,** 206–209 (2008).
23. Bostwick, A., Ohta, T., Seyller, T., Horn, K. & Rotenberg, E. Quasiparticle dynamics in graphene. *Nature Phys.* **3,** 36–40 (2007).
24. Bostwick, A. *et al.* Observation of plasmarons in quasi-freestanding doped graphene. *Science* **328,** 999–1002 (2010).
25. Liu, Y., Willis, R. F., Emtsev, K. V. & Seyller, T. Plasmon dispersion and damping in electrically isolated two-dimensional charge sheets. *Phys. Rev. B* **78,** 201403 (2008).
26. Tegenkamp, C., Pfnur, H., Langer, T., Baringhaus, J. & WSchumacher, H. Plasmon electron-hole resonance in epitaxial graphene. *J. Phys. Condens. Matter* **23,** 012001 (2011).
27. Brar, V. W. *et al.* Observation of carrier-density-dependent many-body effects in graphene via tunneling spectroscopy. *Phys. Rev. Lett.* **104,** 036805 (2010).
28. Cho, J. H. *et al.* Printable ion-gel gate dielectrics for low-voltage polymer thin-film transistors on plastic. *Nature Mater.* **7,** 900–906 (2008).
29. Yamamoto, K., Tani, M. & Hangyo, M. Terahertz time-domain spectroscopy of imidazolium ionic liquids. *J. Phys. Chem. B* **111,** 4854–4859 (2007).
30. Palik, E. D. *Handbook of Optical Constants of Solids* (Elsevier, 1998).
31. Li, X. S. *et al.* Large-area synthesis of high-quality and uniform graphene films on copper foils. *Science* **324,** 1312–1314 (2009).

Acknowledgements

The authors thank R. Sagelman and B. Boudouris for providing the ion gel and X. Zhang for helpful discussions. This work was supported by an Office of Naval Research MURI award (N00014-09-1066 to L.J., J.H., C.G., A.Z. and F.W.) and the Office of Basic Energy Sciences, US Department of Energy (contract nos DE-AC02-05CH11231 for the Materials Science Division to Y.R.S. and F.W. and DE-AC02-05CH11231 for the Advanced Light Source). F.W. also acknowledges support from a Lucile and William Packard fellowship and a Hellman family fellowship, and L.J. acknowledges the support of a Lam fellowship.

Author contributions

F.W. and L.J. conceived the experiment. L.J. carried out optical measurements, B.G., J.H., X.L. and C.G. contributed to sample growth and fabrication, and L.J. and F.W. performed theoretical analysis. All authors discussed the results and wrote the paper.

Additional information

The authors declare no competing financial interests. Supplementary information accompanies this paper at www.nature.com/naturenanotechnology. Reprints and permission information is available online at http://www.nature.com/reprints. Correspondence and requests for materials should be addressed to F.W.